Surface-layer turbulence, energy-balance and links to atmospheric circulations over a mountain glacier in the French Alps.

Maxime Litt[1,2], Jean-Emmanuel Sicart[3], Delphine Six[4,], Patrick Wagnon[3], and Warren D. Helgason[5]

[1]Université Grenoble Alpes, LTHE, F-38000 Grenoble, France
[2]ICIMOD, GPO Box 3226, Kathmandu, Nepal
[3]IRD/Université Grenoble Alpes/CNRS/G-INP, LTHE UMR 5564, Grenoble, France
[4]CNRS, LGGE, F-38000 Grenoble, France
[5]Civil and Geological Engineering, University of Saskatchewan, 57 Campus Drive, Saskatoon S7N 5A9, Saskatchewan, Canada

Correspondence to: M.Litt (maximelitt@gmail.com)

Abstract. Over mountain glaciers, large errors may affect turbulent surface heat fluxes estimated with the bulk-aerodynamic (BA) method. That might lead to uncertainties in estimating melt from surface energy balance (SEB). To characterize the turbulence and the turbulent fluxes, data were collected in the atmospheric surface layer of Saint-Sorlin Glacier (French Alps, 45° N, 6.1° E, ~ 3 km^2). The set-up consisted of high frequency Eddy-Covariance (EC) in 2006 and mean air-temperature and wind-speed vertical profiles in 2009. We studied the influence of the BA method errors on the melt estimations, calculating the SEB alternatively with turbulent fluxes obtained from the BA and the EC methods. We classified our results in terms of large-scale forcing. In weak synoptic forcing, local thermal effects dominated the wind circulation. On the glacier, weak katabatic flows with a wind-speed maximum at low height (2-3 m) were detected 71% of the time and were generally associated with weak turbulent kinetic energy (TKE) and turbulent fluxes. When the large-scale forcing was strong, the wind in the valley aligned with the glacier flow, intense downslope flows were observed, no wind-speed maximum was visible below 5 m, TKE and turbulent fluxes were often intense. For both regimes, the surface layer turbulence production was probably not at equilibrium with dissipation because of the interaction of large-scale orographic disturbances with the flow when the forcing was strong, or low-frequency oscillations of the katabatic flow when the forcing was weak. When TKE was low, all turbulent fluxes calculation methods provided similar fluxes. When TKE was large, the EC method provided larger fluxes than the BA method. This underestimation was compensated by increasing the BA flux estimates using melt-calibrated effective roughness lengths. Though strong forcing was more frequently associated with large TKE events than weak forcing conditions, differences between the different SEB estimates remained in both cases within the error range of observed melt.

1 Introduction

Climate change might affect the hydrological regimes in glacierized mountainous catchments (Viviroli et al., 2011). There is a strong need to understand the links between large-scale atmospheric changes and glacier melt processes. The melt response of glaciers to climate change is generally assessed using calibrated temperature-index models of various complexities (Hock,

2003; Huss et al., 2010; Pellicciotti et al., 2012). Though these models perform correctly when meteorological conditions do not differ much with regard to the calibration period conditions, under changing climate, the frequency of occurrence of specific atmospheric circulation patterns may change (Corti et al., 1999), affecting relationships between temperature and melt. The physical link between glacier melt and climate is the surface energy balance (SEB), embodying all the heat exchanges occurring near the glacier surface (Oke, 1987). Surface energy balance studies under contrasted climatic conditions are required to validate temperature-index calibrations, and adapt them to changing melt processes in a changing climate.

Turbulent energy transfer can play a significant role in the SEB of glaciers (e.g. Sicart et al., 2008; Six et al., 2009) but the fluxes are poorly quantified, since they are usually evaluated using the so-called bulk aerodynamic (BA) method, based on similarity assumptions which state fluxes are constant with height and that turbulent mixing scales with mean vertical gradients of wind speed, temperature and humidity near the surface. These assumptions are frequently violated over mountain glaciers. Vertical flux divergence and non-stationarity of the flow (Denby and Greuell, 2000; McNider, 1982) occurs under katabatic winds, a common feature of air flows above glaciers (Poulos and Zhong, 2008). Non-stationarity of the flow can be induced by the interaction of outer-layer turbulent structures with the surface layer and by the katabatic forcing. Outer-layer structures might be generated when synoptic forcing is strong and the large-scale atmospheric flow interacts with the complex orography (Smeets et al., 1999, 2000). Unmet similarity assumptions may lead to systematic biases in the flux evaluation with the BA method (Mahrt, 2008; Litt et al., 2015a).

The impact of biased turbulent heat fluxes estimates on SEB calculations has been documented for vegetation canopies (Gellens-Meulenberghs, 2005; Stoy et al., 2013), but few studies have dealt with glacier or snow surfaces (e.g. Helgason and Pomeroy, 2012; Conway and Cullen, 2013). Although numerical simulations have shown the BA method was reliable in estimating the surface fluxes in the presence of flux divergence below a wind-speed maximum (Denby and Greuell, 2000), the effects of katabatic oscillations and outer-layer interactions remain poorly documented over mountain glaciers (Smeets et al., 1999, 2000). Evaluating the accuracy of the BA method for different large-scale forcings is necessary to understand the impact of the similarity assumptions on SEB calculations over mountain glaciers, and thus, on the evaluation of glacier melt rates from meteorological measurements or from climate data.

This study on the Saint-Sorlin glacier (French Alps, Grandes Rousses massif, 45° N, 6.1° E) compares turbulent flux measurements with observed large-scale weather patterns over Europe. We investigated the impact of turbulent flux measurement errors on glacier SEB calculations, for different prevailing atmospheric circulation patterns. The study covers two melt periods during the summers of 2006 and 2009, for which dominant atmospheric conditions were contrasted. Atmospheric circulation patterns were characterized with a daily time series of weather patterns derived from the analysis of Garavaglia et al. (2010). Surface-layer flow and turbulence data were obtained from two field campaigns deployed in the ablation area of the glacier. We used data from a 6-m mast measuring vertical profiles of wind speed and temperature in 2009, a high frequency Eddy-Covariance system in 2006, and radiation, temperature, wind speed and humidity measured by automatic weather stations during both campaigns. We characterized the turbulence in the surface-layer over the glacier and calculated the turbulent fluxes with both the BA and EC methods. We used these fluxes together with the measured radiative fluxes to compute the SEB. We

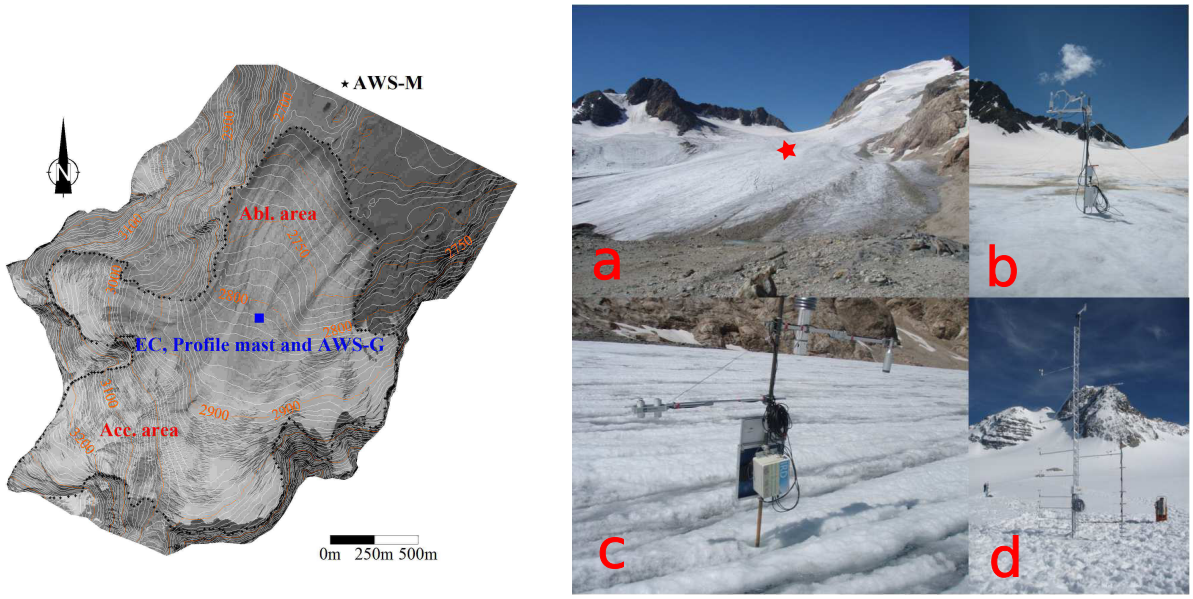

Figure 1. Overview of the glacier and the instruments installed during the field campaigns. (left) Topographic map of the glacier and position of the instruments. (a) Picture of the Saint-Sorlin glacier taken from the AWS-M (heading to the top of the glacier, south is at the horizon), (b-c-d) the instruments installed during the 2006 and 2009 campaigns.

discuss the difference on the SEB calculations resulting from the use of different methods to derive the turbulent fluxes, for the two melt periods.

2 Site and data

2.1 Saint-Sorlin glacier

Saint-Sorlin Glacier is a small mountain glacier (surface area $\simeq$3 km^2.) which altitude ranges between 2700 and 3400 m a.s.l (Fig. 1). It is located in the western part of the French Alps in the Grandes-Rousses massif (Fig. 2). It is characterized by a large flat ablation area (slope $\simeq 5°$) between 2700 and 2900 m a.s.l. Some steep slopes ($> 35°$) are found higher. Ice flows from the South-South-West to the North-North-East, inside a valley which has the same orientation. This valley is bordered by a steep ridge on its western flank and is opened on its eastern flank. The annual mass balance of the glacier has been monitored since 1957 (Vincent et al., 2000; Six and Vincent, 2014). All mass-balance data are available at http://www-lgge.obs.ujf-grenoble.fr/ServiceObs/index.htm.

Table 1. Characteristics of sensors from the automatic weather stations (AWS-G and AWS-M), the eddy-covariance (EC) and the profile mast. We present the random errors on the measurements, as provided by the manufacturer and the random measurement errors that we used to quantify uncertainties on the turbulent fluxes. Minimum and maximum heights refer to the lowest measurement levels in the case of the profile data.

Quantity	Instrument	Precision according to the manufacturer	Accuracy used in this study	Sensor Height (m) Mean	σ	min	max
Profile Mast (2009 campaign)							
Aspirated air temperature, °C	Type-T thermocouple	0.1 °C	0.1 °C	0.74, 0.84, 1.04, 1.24, 1.54, 1.84, 2.44, 3.14, 4.64	0.30	0.20	1.50
Wind speed, m s^{-1}	Vector A100L2	1% of reading	0.1 m s^{-1}	0.83, 1.43, 2.33, 3.03, 4.03	0.30	0.35	1.70
Eddy Covariance System (2006 campaign)							
High frequency wind speed components, m s^{-1}	Campbell C-SAT3	w: ± 0.040 m s^{-1} u, v: ± 0.015 m s^{-1}	$< \pm$ 0.04 m s^{-1} ± 0.015 m s^{-1}	2.37	0.20	2.10	2.95
High frequency sonic temperature, °C	Campbell C-SAT3	0.025°C	0.025°C	2.37	"	"	"
High frequency specific humidity, %	LICOR7500	2% of reading	2% of reading	2.37	"	"	"
Automatic Weather Stations (2006 and 2009 campaigns)							
Aspirated air temperature, °C and relative humidity, %	Vaisala HMP45C	± 0.2 °C 3%	± 0.2 °C 3%	2.30	0.25	1.80	2.70
Wind speed, m s^{-1}	Young 05103	0.3 m s^{-1}	0.3 m s^{-1}	2.50	0.20	2.00	2.95
Wind direction, deg	Young 05103	$\pm 3°$	$\pm 3°$	"	"	"	"
Incident and reflected shortwave radiation, Wm^{-2}	Kipp and Zonen CM3	10% on daily sums	0.4% 0.4%	1.20	0.20	0.80	2.20
Incoming and outgoing longwave radiation, Wm^{-2}	Kipp and Zonen CG3	10% on daily sums	0.4% 0.4%	1.20	0.20	0.80	2.20
Surface elevation changes, m	Campbell SR50	$\pm$ 0.01 m	$\pm$ 0.1 m	1.80	0.20	1.20	2.45

2.2 Field campaigns

We used data from two field campaigns focused on the ablation area of the glacier at around 2800 m a.s.l (Fig. 1). The first campaign was undertaken between 9 July and 28 August 2006, featuring a tower-mounted EC system measuring the three wind-speed components, air temperature and specific humidity at 20 Hz. The second campaign was staged between 13 June and 04

September 2009. We installed 5 cup anemometers and 9 ventilated thermocouples on a 6-m mast, measuring mean temperature and wind-speed profiles. During both campaigns there was an adjacent automatic weather station (AWS-G) consisting of instruments measuring mean aspirated air temperature and humidity, mean wind speed and direction, incoming and outgoing shortwave and longwave radiation fluxes. All masts were fixed into the ice. Height changes due to melt or snow deposition were measured with a sonic height ranger. Due to high melt rates ($\simeq$ 6 cm day^{-1}), the height of the sensors changed with time. Instruments were manually lowered every 10 to 15 days. A picture of the instruments installed on the glacier is shown in Fig. 1. We also used data from an automatic weather station located outside the glacier (AWS-M), on a nearby moraine north of the site (1.5 Km), measuring the same variables as the AWS-G. This station is operated in the framework of the GLACIOCLIM program (les GLACIers, un Observatoire du Climat) that undergoes a follow-up of glaciers mass balance and meteorology in order to understand glacier fluctuations in terms of climatic variations. Table 1 summarizes all the instruments used and their characteristics.

At the beginning of both campaigns, the glacier surface was covered with old winter or spring snow and was smooth (Fig. 1b and d). The glacier surface was irregular at the end of the campaigns due to strong melt that caused the appearance of gullies (Fig. 1a and c). Height changes of about 20 to 30 cm were observed on horizontal scales of about 2-3 m (not shown). The glacier surface characteristics remained homogeneous in every directions on hundreds of meters from the measuring site.

2.3 Data processing

Data have been processed in a similar way than in Litt et al. (2015b). All data were split into 1-h runs. High frequency data from the EC system were checked for quality (Vickers and Mahrt, 1997). Problems were mainly related to precipitation events or frost on the sensor heads. Bad quality runs were discarded (30%). Remaining good-quality runs (GQR) were despiked (Vickers and Mahrt, 1997). A planar-fit rotation (Wilckzak et al., 2001) was applied on each 10 to 15 day period between field visits when they were manually lowered. From this rotation we derived the longitudinal (u), lateral (v) and vertical (w) wind-speed components. The sonic temperature was corrected for water vapour influences (Schotanus et al., 1983). The changes in instrument heights were taken into account using measurements from the sonic height ranger and regular field visits and controls.

3 Methods

3.1 Characterization of large-scale forcing

We characterized the large-scale forcing and the frequency of typical atmospheric circulation patterns during the campaigns using a daily time series of weather patterns (WP). We used the the results of the Garavaglia et al. (2010) WP analysis which is based on the study of the shapes of the precipitation fields measured in the south-east of France, between 1956 and 1996. The shapes of the measured precipitation fields, at the daily time scale, are classified into 8 different classes. For each class, a mean observed geopotential height field over Europe is computed. Then, for any day (inside or outside the period used to

characterize the decomposition, e.g. 1956-1996) the observed geopotential height field shape over Europe is characterized by the observed geopotential height at 0h and 24h, at the 700 hPa level and the 1000 hPa level for 110 grid points (a total of 440 points). This field is compared, in this 440 dimensions space, to the 8 geopotential height fields proposed by the rain-patterns analysis. The nearest of the 8 fields provides the WP. Details of the procedure can be found in Garavaglia et al. (2010).

A WP classification cannot be separated from the object it aims to characterize. An ideal WP decomposition for surface-layer turbulence studies would be based on surface energy flux-related variables such as ground-based measurements of temperature, wind speed or humidity rather than on precipitation. However, the Garavaglia et al. (2010) decomposition is useful here for an exploratory study, in which we use the WP to identify the direction and strength of the large-scale flows, and to obtain a frequency of typical large-scale circulation patterns during each campaign. Large-scale flow direction and strength is related to the displacement of low-pressure systems and thus to the shape of geopotential height fields. Since each WP is associated with a mean geopotential height field shape in the analysis of Garavaglia et al. (2010), it provides a simple and convenient tool for this study. An approximative direction of the atmospheric flow at low level above the ground can be associated with each WP (Fig. 2).

We grouped together the WP for which the wind conditions on the glacier were expected to be similar and we conserved three subsets. Low-pressure systems coming from the West, the South west and South can cause strong winds aligned with the valley and the glacier flow (Fig. 2). These conditions are related to Atlantic waves, South-west and South Circulations and Central Depressions. We grouped together the corresponding WP (patterns 1, 3, 4 and 7, Garavaglia et al., 2010) in a Strong Forcing (SF) subset. Large-scale flows associated with WP1 are not well aligned with the glacier (Fig. 2). Nevertheless for this WP we observe strong downslope flows above the glacier. We refer to weak large-scale flows, related to the presence of high-pressure systems (WP8) as Weak Forcing (WF). The WP 2, 5 and 6 are associated with Steady Oceanic Circulations, East Returns and North-east Circulations, respectively, and are grouped together as Other Forcing (OF). They present very distinct characteristics in terms of large-scale flow directions. They are generally associated with precipitation events or freezing, low wind speeds and erratic wind directions on the glacier, thus only a small fraction of the corresponding runs are classified as good-quality runs (Table 2) and we do not analyze them in detail herein.

3.2 Turbulence characteristics of the surface flow

High-frequency measurements were undertaken at low height ($\sim$2 m), supposedly inside the surface layer, which is defined as the layer of air above the surface for which the turbulent fluxes do not change by more than 10% of their surface values (Stull, 1988). Monin-Obukhov Similarity Theory (herein, MOST, Monin and Obukhov, 1954), which underlies the BA method, assumes that the production of turbulent kinetic energy (TKE) in the stable surface layer is related to the mean local shear. The production of turbulence must be balanced by buoyancy and by destruction by viscous dissipation. No turbulent energy must be transported from the outer layers towards the surface layer and no advection shall transfer turbulence from some other parts of the field (Monin and Obukhov, 1954). To study the intensity of the turbulence in relation with the WPs, we computed the mean TKE ($\overline{e}$) using the EC data (overlines indicate temporal averages over a 1-h run and primes denote fluctuations around

this mean):

$$\overline{e} = \frac{1}{2}\left(\overline{u'^2} + \overline{v'^2} + \overline{w'^2}\right), \quad (1)$$

with u, v and w the longitudinal, lateral and vertical wind speed components, respectively. Spectral analysis permits a characterization of the turbulent flows. We used it to assess the validity of MOST, assuming that in an equilibrium surface layer, turbulent spectra and cospectra should compare well with the Kansas curves (Kaimal et al., 1972) measured under ideal conditions, and that deviations from these curves are expected if the surface layer is not in equilibrium. We studied the Fourier spectra (S) of the wind-speed components and the cospectra (Co) of u with w (associated with turbulent momentum flux) and of w with the potential temperature, θ (sensible heat), and with the specific humidity, q (latent heat). Following Smeets et al. (1999), individual spectra were normalized by the variance of w which led to a collapse of individual curves at high frequency. Heat flux-related cospectra were normalized by the kinematic flux ($\overline{w'\theta'}$ or $\overline{w'q'}$). We did not normalize Co_{uw} since $\overline{u'w'}$ is expected to be small and erratic near a wind-speed maximum as observed in katabatic flows. Medians of spectral powers over subsets of runs were calculated on equally spaced logarithmic intervals

The turbulent fluxes of sensible (H) and latent heat (LE) can be written as:

$$H = -\rho C_p \overline{w'\theta'}_s = -\rho C_p u_* T_*, \quad (2)$$

$$LE = -\rho L_e \overline{w'q'}_s = -\rho L_e u_* q_*, \quad (3)$$

where fluxes directed towards the surface and towards the atmosphere are defined as positive and negative, respectively. The symbols u_*, θ_* and q_* stand for turbulent velocity, temperature and humidity surface-layer scales. The subscript s refers to surface values, ρ is the air density ($kg\ m^{-3}$), C_p is the specific heat of humid air (1003.5 $J\ kg^{-1}\ K^{-1}$), L_e is the latent heat of sublimation of the ice ($2.83 \times 10^6\ J\ kg^{-1}$) when the surface is below freezing and the latent heat of vaporization ($2.50 \times 10^6\ J\ kg^{-1}$) when the surface is melting and k is the von-Karman constant (0.4). To apply Equations 2 and 3 we used alternately the BA and the EC methods (subscript b and EC refer to the BA or the EC method, respectively). The EC method relies on direct measurements of the fluctuating quantities u, θ and q, at some height above the surface, assuming fluxes are constant between the surface and this level. The BA method estimates u_*, θ_* and q_* using finite differences of mean measurements between the sensors and the surface, assuming that the fluxes scale with the mean vertical gradients:

$$u_{*_b} = k\frac{\overline{u}}{\left(\ln\left(\frac{z}{z_0}\right) - \psi_m\left(\frac{z}{L_*}\right)\right)} \quad (4)$$

$$\theta_{*_b} = k\frac{(\overline{\theta} - \overline{\theta}_s)}{\left(\ln\left(\frac{z}{z_t}\right) - \psi_t\left(\frac{z}{L_*}\right)\right)} \quad (5)$$

$$q_{*b} = k\frac{(\overline{q} - \overline{q}_s)}{\left(\ln\left(\frac{z}{z_q}\right) - \psi_q\left(\frac{z}{L_*}\right)\right)} \quad (6)$$

The length scales z_0, z_t and z_q are the dynamical, thermal and humidity roughness lengths (m), respectively. They were evaluated by least square iterative fitting of the temperature and wind speed vertical profiles measured in 2009, and assuming $z_q = z_t$. When we use these roughness lengths to model the fluxes, the method is referred to as $\mathrm{BA_{pro}}$. The method for roughness length determination was inspired from Andreas (2002) and developed for the tropical Zongo glacier. It is detailed in (Sicart et al., 2014). The results show a large scatter, about four orders of magnitude. The median values are $z_0 = 0.001$ m and $z_t = 0.00001$ m. The scatter can be attributed to poor accuracy of the temperature measurements leading to large random uncertainties (Sicart et al., 2014). The scatter was too large to observe significant changes in the measured roughness lengths during the 2009 campaign, in spite of snow falls or snow melt that uncovered the ice surface, or appearance of small gullies of about 0.1-0.3 m height variations on a few meters horizontal scale that could also have impacted the roughness length (Smeets and Van den Broeke, 2008a, b).

The state of the surface was similar in 2006 and 2009, and we used the same values for the roughness lengths for both field campaigns. In many studies, in order for the SEB to match the measured ablation, turbulent fluxes are adjusted using an effective roughness length z_e such as $z_0 = z_t = z_q = z_e$. This z_e is often larger than the actual aerodynamic values of the roughness lengths (Wagnon et al., 2003; Favier et al., 2004; Cullen et al., 2007; Six et al., 2009). We also computed the BA fluxes using an effective roughness parameter. We set z_e to 0.001 m, calibrated in Six et al. (2009) so that the SEB matches the observed melt during the 2006 campaign. The fluxes modeled like this are referred to as $\mathrm{BA_{eff}}$ fluxes.

We also evaluated the roughness length using the EC system and inverting equations 4 and 5, and selecting neutral runs. The median z_0 was 0.022 m, and the results for z_t was 6.6×10^{-6} m. We did not use these values to calculate fluxes through the BA method.

Stability corrections $\psi_{m,h,q}$, for (m) momentum, (h) temperature and (q) humidity, respectively, were taken from Businger et al. (1971) and Dyer (1974). Temperature of the surface was derived from the outgoing longwave radiation measured at the AWS-G, assuming an emissivity of 0.99 for the ice or snow. Melt was observed most of the time, so that surface temperature was generally 0°C. The value of q_s was derived from the surface temperature assuming air at the surface was saturated. The length scale L_* is the Obukhov length defined as:

$$L_* = -\frac{\overline{\theta} u_*^2}{kg\theta_*} \tag{7}$$

The dimensionless z/L_* is a scaling parameter in the surface layer. When evaluated with the BA method, this parameter documents the stability of the layer of air between the surface and the sensor assuming TKE production scales only on the mean local vertical gradients of wind speed and temperature. The evaluation of Equations 4, 5 and 6 requires an iterative scheme. A first evaluation of u_{*_b}, θ_{*_b} and q_{*b} was obtained assuming neutral stability ($z/L_{*b} = 0$). These estimates were used to compute a value of z/L_{*b}, which was used to calculate a new estimation of u_{*_b}, θ_{*_b} and q_{*b}, and so on, until convergence was reached.

3.3 Errors on turbulent fluxes

We evaluated the random errors on the turbulent fluxes following the methods that Litt et al. (2015a) applied on the Zongo glacier. For the BA method, an analytical calculation was performed, propagating the uncertainties in the measurements of the meteorological variables (Table 1) through Equations 2 and 3. We calculated the uncertainties on the roughness lengths were $\delta \ln z_{0,t,q} \simeq 1.5$ (Sect. 3.2), following Sicart et al. (2014). This error corresponds to the standard deviation of profile-derived roughness lengths. We assumed the errors on the measurements of individual variables were independent and that stability functions did not change much under small variations of the measurements. Surface temperature error depends on the error on LW_{out} which was assumed to be 0.4%: this corresponds to the observed dispersion of the night time measurements of SW_{in} and day time melt conditions measurements of LW_{out}. This method provides much realistic errors on surface temperature ($\sim 0.35°K$) than when using the nominal error on radiation of 10% (leading to errors of 6-7$°K$, Litt et al., 2015a). The largest source of random error was the uncertainty on the roughness lengths, which were not precisely defined

For the EC method, we followed Litt et al. (2015a), assuming measurement uncertainties on wind speed and temperature were negligible and that most random errors were due to insufficient statistical sampling of the largest eddies (Vickers and Mahrt, 1997). We applied the Mann and Lenschow (1994) method which relates the random error to the time scale τ of the largest eddies of the flow. This timescale was derived from the peaks of the cospectra of w with θ and q obtained by Fourier analysis (Wyngaard, 1973).

3.4 Surface energy balance and melt

The melt rate was derived from the surface height changes measured with the SR50 sonic height ranger (h). We assumed the ice density was 900 kg m^{-3}. At the beginning of the campaigns, old snow was present at the surface, with measured density of 480 kg m^{-3}. The precipitated water equivalent during occasional snowfalls on the glacier were obtained from SAFRAN reanalysis data (Durand et al., 1993). The SEB was compared to the melt energy (Melt_i) derived from surface height (h) changes:

$$\mathrm{SEB} = \sum_{day} (SW_{inc} - SW_{out} + LW_{inc} - LW_{out} + H + LE) \tag{8}$$

$$\mathrm{Melt}_i = (h(i+1) - h(i)) \times \rho_s L_f \tag{9}$$

Where i is a daily index, ρ_s is the density of the underlying snow or ice surface (kg m^{-3}), L_f is the latent heat of fusion of ice (3.34×10^5 J kg^{-1}). All fluxes are expressed in W m^{-2}. The symbols SW and LW stand for hourly mean shortwave and longwave radiation, respectively. The subscripts inc and out stand for incoming and outgoing radiation, respectively. Sub-surface conductive heat flux was neglected because the surface remained close to melting day and night ($T_s > -3$°C). A simulation of the conduction flux below the snow or ice surface, using the surface temperature as the only input data, showed that this flux was negligible, even when surface temperature fell below zero during short periods of a few hours. The rare events of strong surface cooling, with surface temperature reaching ~ -11°C during the night, were associated with

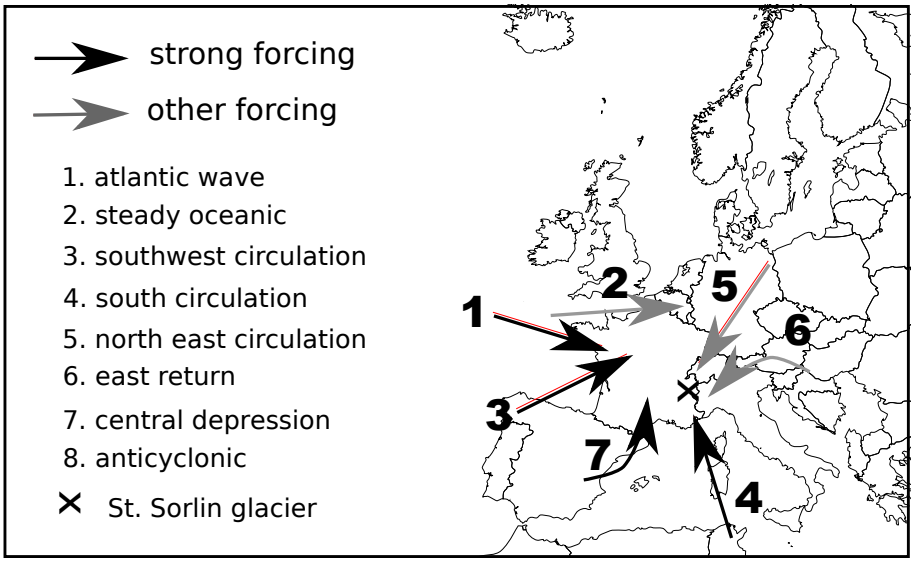

Figure 2. Direction of the atmospheric flow in the lower atmospheric layers for different WP (adapted from Garavaglia et al., 2010). (black arrows) Direction of the flow for the WP associated with SF and (grey arrows) direction of the flow for the other WP. No flow direction is shown for WF conditions (WP8) since atmospheric wind speed was weak and direction ill-defined for these conditions.

precipitation events or freezing for which meteorological data quality was low due to frost or snow deposition on the sensors. These periods were discarded by the quality check procedure. Energy gains due to precipitation are generally negligible for alpine glaciers with significant mass turnover and low rain precipitation intensities (Paterson and Cuffey, 1994; Six et al., 2009; Oerlemans, 2001; Oerlemans et al., 2009). Turbulent fluxes were obtained alternately from the BA_{pro}, the BA_{pro} or the EC methods. Ablation due to evaporation or sublimation at the surface was considered negligible: mean absolute latent heat fluxes remained below 10 Wm^{-2} for the most turbulent subsets (Table 3), which corresponds to a daily ablation of only 0.3 mm w.e. We assumed the error on the measured daily melt was of the order of the SR50 error, i.e. ± 0.01 m, which results in a 40 Wm^{-2} error on the mean hourly melt energy.

4 Results

4.1 Meteorology and wind regimes

We describe the meteorological conditions of each campaign in terms of frequency of SF and WF conditions (Fig. 3). We observed two types of conditions associated with WF weather patterns. One was characterized with high mean temperatures (> 5°C), clear morning skies ($SW_{inc} > 500$ W m^{-2}) with clouds developing in the afternoon (LW_{inc}>300 W m^{-2}), moderate wind speed (3 to 5 m s^{-1}) and wet air (Table 2), as observed during the long WF event at the beginning of the 2006 campaign. The other type of conditions associated with WF was characterized by low temperatures (0-5 °C), covered sky, occasional snow

Table 2. Characteristics of the two field campaigns in terms of WP frequencies, meteorological data and turbulent kinetic energy: Fraction of runs recorded under each group of WPs, and TKE classification. Fraction of good-quality runs for the EC data in 2006, inside each group, and fraction of runs, inside each group during the 2009 campaign, for which a wind-speed maximum was observed with the profile mast. Mean meteorological variables recorded by the AWS-M, mean TKE in each weather group , and fraction of run in SF and WF conditions for which TKE is > 2 ms^{-2} or < 1 ms^{-2}

	Strong Forcing		Weak forcing		2006-TKE	
	2006	2009	2006	2009	$\overline{e} < 1$ ms^{-2}	$\overline{e} > 2$ ms^{-2}
Time coverage	26%	46%	47%	33%	44%	38%
Fraction of good-quality runs (EC)	85%	-	75%	-	49%	29%
Fraction of good-quality runs with a detected wind-speed maximum	-	31%	-	71%%	-	-
Fraction of runs in SF					28%	52%
Fraction of runs in WF					68%	11%
u_{AWS-M} [m s^{-1}]	5.2	5.5	2.5	2.6	2.6	4.4
T_{AWS-M} [°C]	7.2	9.1	7.6	5.3	6.7	5.7
q_{AWS-M} [10^{-3} kg kg^{-1}]	4.9	4.8	5.8	4.9	5.0	4.9
TKE [m^{-2} s^{-2}]	2.6	-	1.0	-	0.52	3.66

falls (nit shown) and low wind speed (2-3 m s^{-1}) and dryer air. This was observed between 10 June and 25 June 2009. The WF patterns are associated with high-pressure systems and to weak synoptic forcing. As a result the valley circulation seemed controlled by local thermal effects. On the glacier, wind blew mostly downslope, day and night (Fig. 4). Upslope winds were observed only 5% of the time. Over the glacier, the local katabatic forcing was dominant: a weak wind-speed maximum was observed at low heights (~ 2 m s^{-1} at ~ 2 m, Fig. 5) for $\sim 70\%$ of the 2009 WF situations (Table 2). During the day, convection probably drove the circulation in the valley: outside the glacier, the wind blew down the valley during the night and up the valley during the day (Fig. 4). The TKE was generally small in these situations (Table 2).

SF conditions were characterized by high wind speeds (peaks above > 7 m s^{-1}), moderate air temperatures (~ 5°C), and generally cloud covered conditions. Such conditions were observed around mid-august in 2006 and mid-July in 2009. SF conditions are related to low-pressure atmospheric system associated with West, South-west or South circulations, roughly aligned with the glacier flow and with the valley. As a result, in the vicinity of the glacier, these conditions were associated with the largest wind speeds, and they seemed to trigger a dominant down-valley circulation, overwhelming convective circulations: on the glacier, wind was blowing downslope 99% of the time (Fig. 4). Day and night, the wind direction was similar over the glacier and outside the glacier. The median wind-speed profiles were nearly logarithmic below 2 m, and the temperature

Table 3. Characteristics of the two field campaigns in terms of turbulent fluxes measured with the EC and modeled with the BA methods with different roughness parameters. Correlation coefficients as well as linear fit parameters between each BA method fluxes and EC fluxes are presented.

	Strong Forcing		Weak forcing		2006-TKE	
	2006	2009	2006	2009	$\overline{e} < 1$ ms^{-2}	$\overline{e} > 2$ ms^{-2}
Fluxes [W m^{-2}]						
H_{EC}	45±2	-	24±1	-	18±1	**47**±2
LE_{EC}	-9±3	-	6±1	-	4±1	-10±4
$H_b(z_{0,t,q})$	36±1	47±1	18±1	9±1	18±1	**34**±1
r	0.60		0.33		0.67	**0.41**
$y = ax + b$	$0.57x + 11$		0.34x+11		0.61x+7.82	**0.68x+1.59**
$LE_b(z_{0,t,q})$	3±1	3±1	6±1	-1±1	5±1	-2±1
r	0.04		0.05		-0.06	0.10
$y = ax + b$	-0.04x-3		0.05x+6		0.12x+4.41	-0.05x-2.2
$H_b(z_e)$	50±2	66±3	20±1	7±1	21±1	**47**±2
r	0.60		0.25		0.32	**0.66**
$y = ax + b$	0.88x+10		0.37x+13		0.65x+9.05	**1.05x-2.61**
$LE_b(z_e)$	-6±2	4±1	7±1	-3±1	5±1	-5±2
r	-0.03		0.03		-0.06	0.09
$y = ax + b$	-0.05x-6		0.03x+7		0.15x+4.12	-0.08x-5

inversion was marked (Fig. 5). A katabatic wind-speed maximum was not frequently observed at low heights (Table 2 and Fig. 5), either because it was located above the mast, or hidden in the background flow, or inexistent. The TKE was generally high (Table 2) for these conditions.

4.2 Turbulent characteristics of the surface flow

4.2.1 Turbulent kinetic energy

For WF and SF conditions, TKE generally was low and high, respectively. However, some high and low TKE cases remained in the classification (Table 2). In the following, we thus characterized the surface layer flow by selecting 2 subsets of runs of

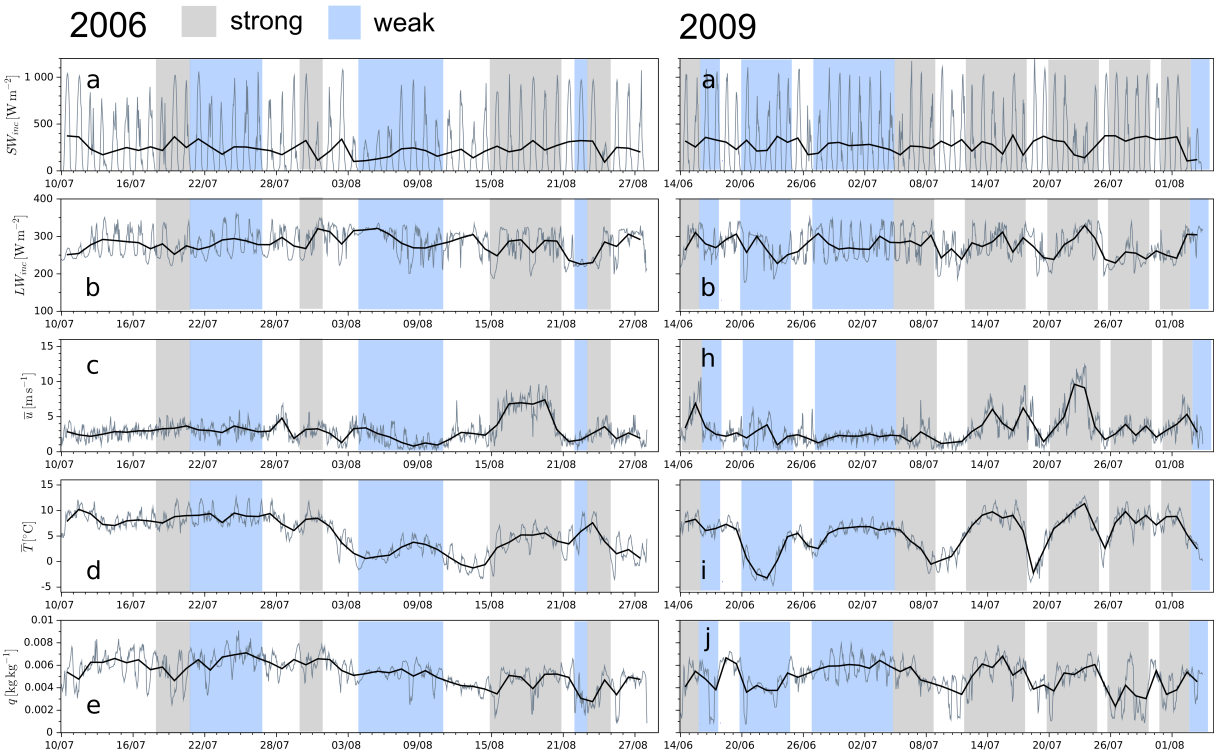

Figure 3. Change of the meteorological variables in the ablation zone of the glacier at the AWS-G in (left) 2006 and (right) 2009. (a-f) incoming shortwave radiation, (b-g) incoming longwave radiation, (c-h) wind speed, (d-i) air temperature and (e-j) specific humidity of the air. SF conditions are dark shaded and WF conditions are light shaded. The gray lines in lower panels (c, d, e, h. i and j) show daily averages.

the EC data of 2006 that exhibited contrasted TKE range in order to select runs presenting similar turbulence characteristics. We analysed the most frequent runs for which wind blew downslope (direction between 90° and 270°, 85 % of the GQR), keeping only cases for which $H_{EC} < -5$ W m^{-2} and $\overline{u} > 2$ m s^{-1} in order to filter for cases when turbulence was sufficiently developed. We separated these runs in two subsets, one for which TKE was high, requiring $\overline{e} > 2$ m^2 s^{-2} (14% of the GQR) and a subset for which TKE was low, with $\overline{e} < 1$ m^2 s^{-2} (31% of the GQR). This classification distinguishes typical turbulent conditions and groups together spectra and cospectra of similar shapes (Sect. 4.2.2). We then discuss the characteristics of the WP classes, remembering that 52% of SF conditions show $\overline{e} > 2$ m^2 s^{-2} and 67 % of the WF conditions show $\overline{e} < 1$ m^2 s^{-2}.

4.2.2 Spectral analysis

The Fourier analysis of the 2006 EC wind speed components and temperature data was compared to the Kansas curves, to see if the surface layer was in equilibrium (Sect. 3.2). Wind speed spectra in Fig. 6a and 6b show that the horizontal and the vertical wind speed oscillated at low frequency, more than expected for an equilibrium surface layer. For $n < 10^{-1}$ the horizontal and vertical wind-speed spectra were higher than the prediction of Kaimal et al. (1972) for the z/L_* measured with

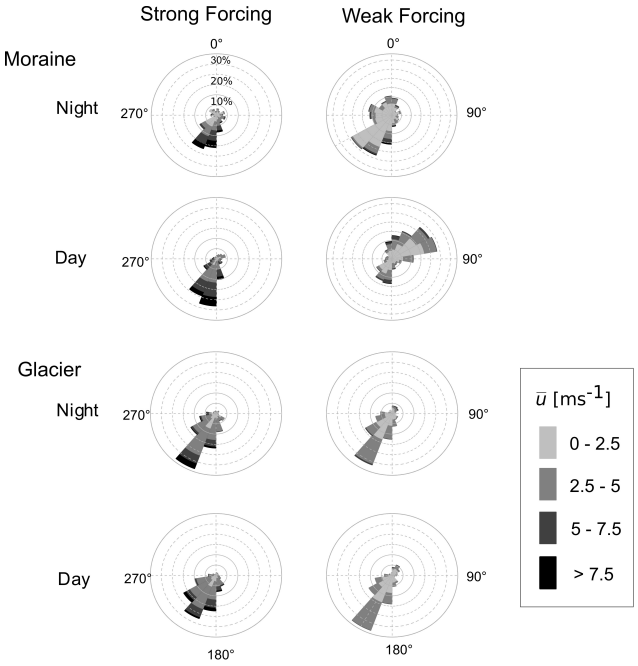

Figure 4. Rose diagrams of wind direction and speed measured by the AWS-G and the AWS-M for Strong (left panels) and Weak (right panels) Forcing conditions during the night (upper panels) and during the day (lower panels) .

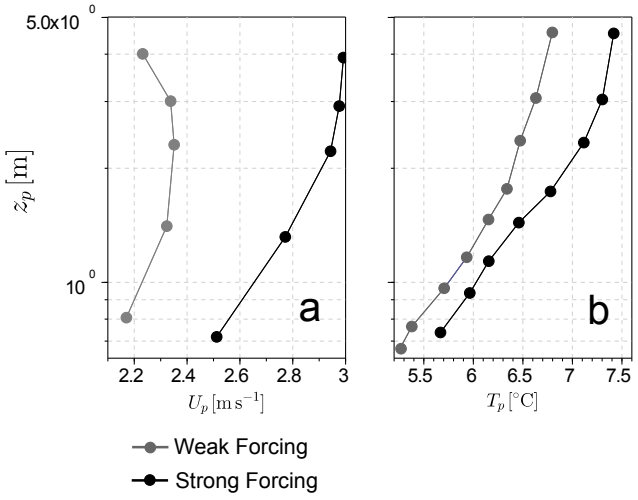

Figure 5. (a) Median wind-speed profiles and (b) temperature profiles during the 2009 field campaign for (gray) WF conditions and (black) SF conditions.

the EC method in the surface layer. The amplitude of these low-frequency oscillations was much larger for the longitudinal

than for the vertical wind speed. Similar observations were made for large and low TKE runs, except that the peak in S_u was observed at $n \sim 5 \times 10^{-2}$ and $n \sim 5 \times 10^{-3}$ when $\overline{e}$ was high and low, respectively.

The low-frequency oscillations of u and w affected the momentum flux. For high $\overline{e}$ and $n > 10^{-2}$ the median cospectrum of w with u was negative (Fig. 6d). For $n < 10^{-2}$ the median cospectrum reversed its sign, a peak was observed at the same frequency as the low-frequency peak of S_u ($n \sim 5 \times 10^{-2}$), and the dispersion between the individual cospectra was large. When $\overline{e}$ was low, Co_{uw} was low too. For $n > 10^{-2}$ the median cospectrum was slightly positive, indicating an upward momentum flux, which could be explained by the presence of a katabatic wind-speed maximum just below the sensor, roughly at 2 m above the ground (Fig. 5). For $n < 10^{-2}$ the median cospectra was low, but the individual cospectra were dispersed around zero (hardly visible in Fig. 6d)

Low-frequency oscillations also influenced the sensible (Fig. 6c) and the latent heat fluxes (not shown). When $\overline{e}$ was high, all the individual cospectrum collapsed to a single curve and the dispersion was low. The median cospectrum exhibited a small plateau at the frequency of the peak in the Kansas curve. A peak was observed above the Kansas curve at $n \sim 5 \times 10^{-1}$. For $n < 5 \times 10^{-1}$, the median cospectrum fell to zero. When $\overline{e}$ was low, the dispersion between the individual cospectra was high. The median cospectrum peaked at the frequency of the peak in the Kansas curve ($n \sim 5 \times 10^{-1}$). For $n < 5 \times 10^{-1}$ the median cospectra fell to zero erratically. At the lowest frequency end, individual cospectra were dispersed around zero.

4.2.3 Turbulent fluxes

Low TKE cases were characterized by low and positive sensible heat fluxes H (Table 3). The latent heat flux LE was slightly positive too, and net fluxes were a small gain of energy at the surface. Calculating the fluxes with each method did not provide significantly different results on average, even though the BA method results were dispersed (Fig. 7). When TKE was high, H was highly positive, and LE was slightly negative on average, net fluxes were a larger gain of energy for the surface than in low TKE cases. The $\mathrm{BA_{pro}}$ method underestimated the magnitude of H_{EC}, L_{EC} and their sum on average. Random errors were too low too explain such a discrepancy. Results for H correlated with H_{EC} while for LE they were scattered, as a result of large random errors on both methods at the hourly time scale. The use of the $\mathrm{BA_{eff}}$ method provided significantly better correlations with the EC and average magnitudes compared better.

For WF conditions, mainly composed of low TKE runs, the fluxes from each method evolved similarly as for the low TKE subset. The sensible heat flux H was moderately positive, around 20 W $\mathrm{m^{-2}}$, similarly as for the low TKE subset (Table 3). The latent heat flux was a small gain of energy for the glacier, a few W $\mathrm{m^{-2}}$ on average. The resulting net turbulent fluxes were moderately positive. Sensible heat fluxes H when evaluated with the BA were poorly related to the measures (Table 3). Comparison results for LE were highly dispersed, but similar average values were found with the different methods (small on average).

For SF conditions, mainly composed of high TKE runs, the fluxes from each method evolved similarly as for the high TKE subset. The sensible heat flux was significantly positive, around 45 W $\mathrm{m^{-2}}$ on average in 2006. The latent heat flux was negative and stronger in magnitude than in WF conditions, but still low in absolute terms, around -10 W $\mathrm{m^{-2}}$ on average in

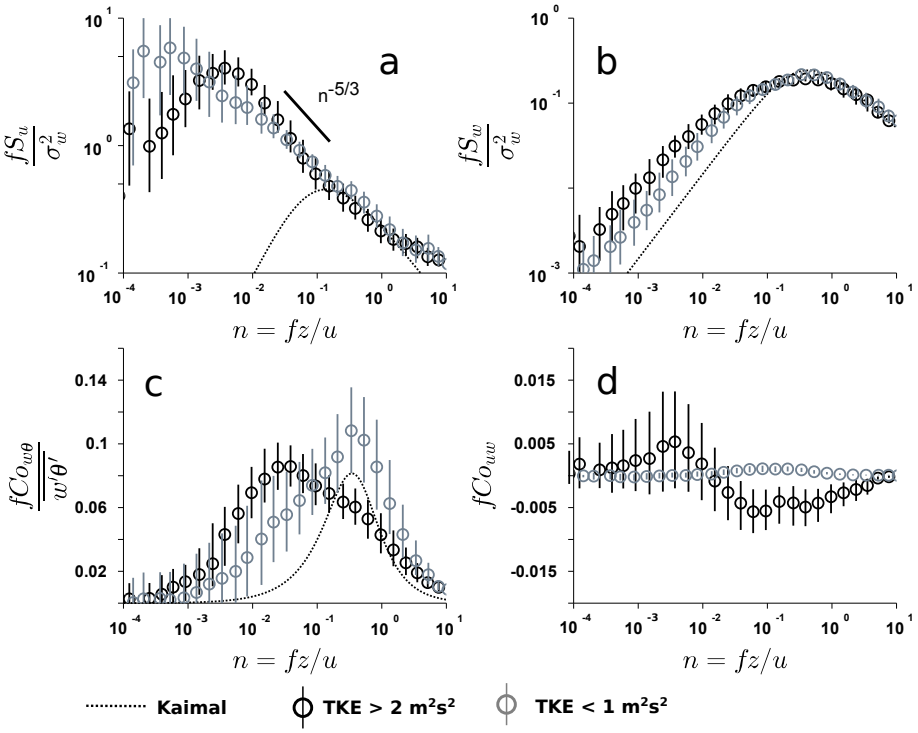

Figure 6. Fourier analysis of the high frequency EC data during the 2006 campaign. The median spectra and cospectra calculated over (black) the high TKE and (grey) the low TKE subsets are presented together with (black dotted) the Kaimal et al. (1972) curve. (circles) average of the spectra or cospectra over a bin of normalized frequency and (vertical bars) interquartile range of the spectra or cospectra over the same bin. (a) Spectra of longitudinal wind speed u, (b) spectra of w, (c) cospectra of w with θ and (d) cospectra of w with u.

2006. Sensible heat fluxes were underestimated with $\mathrm{BA_{pro}}$, but better correlation and less underestimates were found with $\mathrm{BA_{eff}}$ (Table 3). Latent heat fluxes were highly scattered but on average similar in between the different methods.

5 Discussion

5.1 Turbulence in the surface layer.

When the TKE was high, which was observed for 52% of SF conditions, the characteristics of the wind-speed spectra were similar to that of a surface layer influenced by outer-layer turbulence: the variance of u was strongly enhanced at low frequency compared to what is expected for an equilibrium surface layer, while a limited increase was observed in the w spectra, a combination of observations which agrees with the parametrizations of Högström et al. (2002) for surface layers disturbed by large eddies. In the vicinity of the surface, if large-scale structures are transported from the outer-layer, they are supposedly elongated horizontally due to the surface blocking, and due to the large shear in the surface layer. As a result, they must induce large horizontal fluctuations of the horizontal wind speed while the vertical wind speed must be less affected. Also, a

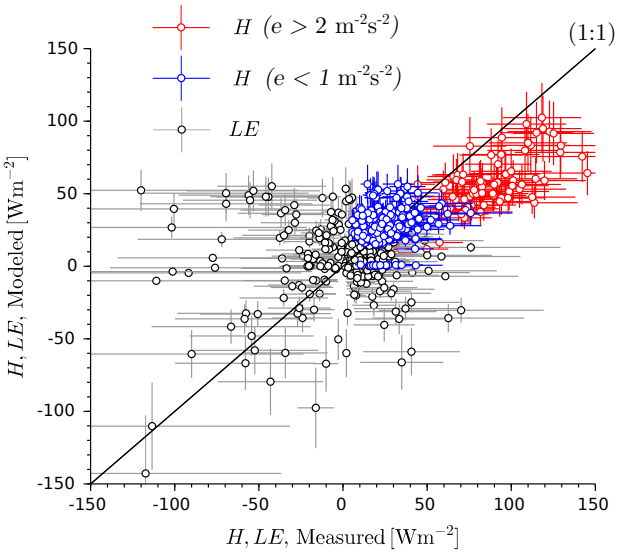

Figure 7. Comparison of hourly fluxes modeled with the BA method and profile-derived roughness length with the fluxes measured with the EC method, for the 2006 field campaign. Red and blue circles show sensible heat fluxes results during the SF event between 16 August and 20 August when TKE was high, and the WF event between 10 July and 26 July when TKE was low, respectively. Black dots are the latent heat fluxes for both cases. Vertical and horizontal bars indicate the random error values.

$n^{-5/3}$ slope was observed on the low frequency part of the u spectra when TKE was large (Fig. 6a). This signature resembles that of an outer, well-mixed layer (Højstrup, 1982). Similar spectral shapes were observed over other mountain glaciers when synoptic forcing was strong (Smeets et al., 1999; Litt et al., 2015b). In these studies, the observed low-frequency oscillations were attributed to the interaction of large scale coherent structures with the surface-layer turbulence. Such structures can be generated when the large-scale flow interacts with the complex mountain orography. In such situations, Smeets et al. (1999) showed that the TKE transport term is not negligible. Significant TKE can be transported from the outer layer and the surface layer turbulence was not in equilibrium with local production. We hypothetise that these kinds of structures were influencing the surface flow on Saint-Sorlin glacier.

Perturbations of the surface layer seemed to have a strong effect on the momentum flux, as shown by the cospectra of u and w, which exhibited erratic contributions around zero at low frequencies (Fig. 6). The perturbations also affected the turbulent heat fluxes, since the cospectra of w with θ peaked and contained more energy at low frequency than the Kaimal predictions. These perturbations likely originated from various turbulent structures sharing similar time scales, since the low frequency peak was observed systematically at $n \sim 10^{-2}$. The influence of these structures on the fluxes was always of the same sign and induced larger heat fluxes magnitudes than predicted by the Kansas curve. The EC method fluxes included the additional fluxes induced by these structures, whereas the BA method could not take it into account since part of the turbulent mixing was not due to local shear production or buoyancy effects. This explains why the $\mathrm{BA_{pro}}$ method systematically underestimated

the fluxes in these conditions (Table 3), and why random errors were too low to explain the observed difference between the fluxes derived from each method. Using the $BA_{\rm eff}$ method provided larger fluxes, that compared better to the EC fluxes, than using the $BA_{\rm pro}$ method (Table 3). This suggests that the use in SEB models of an effective roughness length, larger than the profile-derived dynamic or thermal roughness lengths, respectively, in order to increase the turbulent fluxes so that the SEB matches the melt, is actually a way to compensate potential biases in the BA turbulent fluxes due to failure of the MOST when TKE is high. This is supported by the values of the EC derived roughness lengths, considering they account for the additional mixing: the denominator ($\ln(z/z_0)\ln(z/z_t)$) in the bulk formulation of the fluxes, calculated with the EC derived roughness length or the effective roughness length is roughly identical (0.0165 and 0.0167).

When the TKE was small, which was observed for 68% of WF conditions, low-frequency oscillations of the wind speed were common (Fig. 6). These cases would have favored the development of katabatic flows, which lead to vertical flux divergence and to a deconnection of turbulence characteristics below and above the wind-speed maximum height. The surface layer is limited to a small fraction of the wind speed maximum height (Denby and Greuell, 2000). Katabatic flow oscillations, inducing periodic oscillations of the wind-speed and the katabatic layer depth, are also a common feature of katabatic flows (McNider, 1982). The cospectra of w with u was slightly positive (Fig. 6d), suggesting the wind maximum was most of the time just below the EC system, in agreement with the the average observed wind maximum height of the 2009 campaign for WF conditions (Fig. 5). Assuming the flow oscillated, the depth of the katabatic layer and the height of the wind-speed maximum oscillated too, shifting from above to below the EC system. This explains the presence of low frequency contributions in the wind speed spectra, and the erratic behaviour of the cospectra of w with θ at low frequencies (Fig. 6): changes in the depth of the katabatic layer provoked an erratic divergence of the fluxes in the first meters above the surface. The concept of a surface layer was maybe not even relevant below a wind speed maximum at less than 1.5 m. As a result, the fluxes from the BA method and the EC method evaluated at a 2-m height were decorrelated (Table 3).

5.2 Surface energy balance and melt

During both campaigns, the SEB was mainly controlled by large radiative fluxes, regardless of large-scale forcing, but the contribution of turbulent fluxes to the SEB was significant (Fig. 8). Random errors on turbulent fluxes remained small in comparison with the total SEB. All SEB calculations compared well with the sonic height ranger measurements within the estimated error range. Yet, changes in net turbulent fluxes resulting from the choice of calculation method remained too small in comparison with the radiative balance to yield significant differences in the SEB estimates.

Weak forcing conditions dominated during the 2006 campaign (Table 2), and the mean net turbulent fluxes were moderate (~ 25 Wm^{-2}). Since TKE was generally low for these conditions, small differences were observed between turbulent fluxes derived with different calculation methods, compared to the large radiative inputs (Fig. 8). In 2009 for these conditions, turbulent fluxes were nearly negligible (< 10 Wm^{-2}), and the difference between them was too low in absolute terms to yield significant differences in the calculated SEB.

Since TKE was generally large in SF conditions, one would have expected the EC method to provide larger turbulent fluxes than the BA method (Sect. 4.2). Nevertheless, for SF conditions in 2006, all turbulent fluxes calculation methods provided

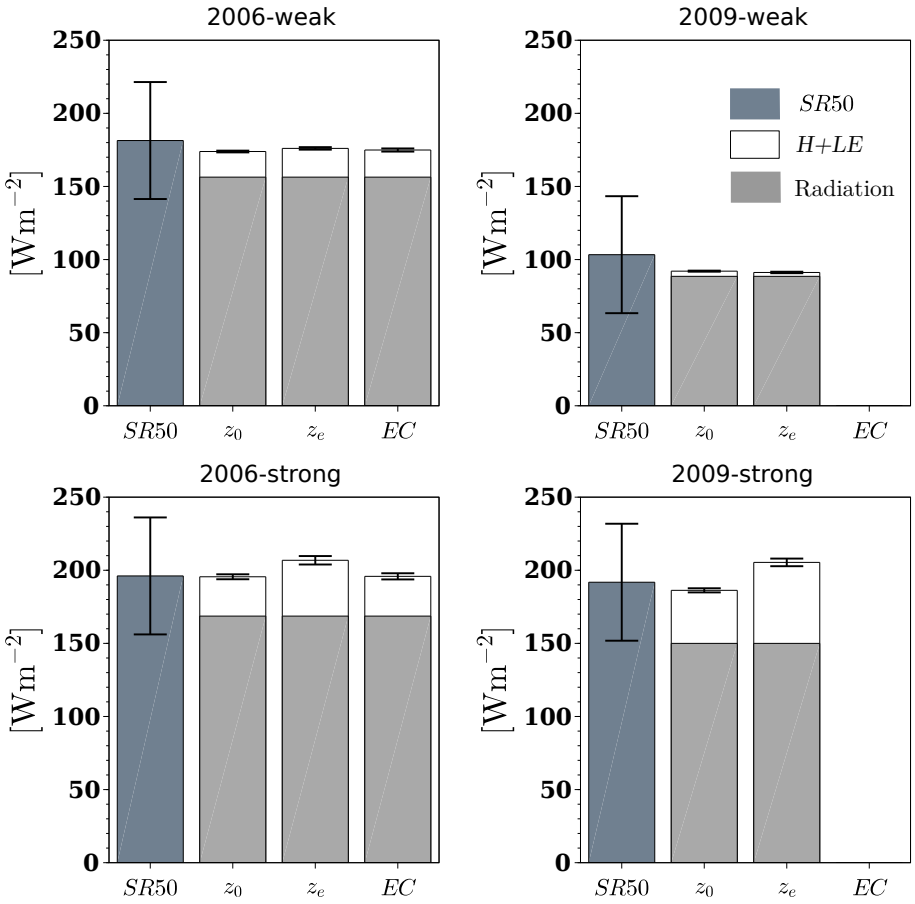

Figure 8. Mean measured melt and SEB for (a and b) WF and (c and d) SF conditions, during (a and c) 2006 and (b and d) 2009 campaigns. (gray) radiation balance, (dark grey) melt measured by the SR50 and (whitw) net turbulent flux ($H + LE$) evaluated with the $\mathrm{BA_{pro}}$ method, with the $\mathrm{BA_{eff}}$ method and with the EC method. Random error on turbulent fluxes and a 40 $\mathrm{Wm^{-2}}$ interval for the melt energy derived from the SR50 measurements are shown by the black error bars.

similar mean turbulent fluxes (~ 35 $\mathrm{Wm^{-2}}$). This could be explained by the presence of low TKE runs in these conditions, for which the discrepancies between turbulent flux calculation methods were small. In 2009 for SF conditions, the difference between the SEB calculations was high (Fig. 8d), the $\mathrm{BA_{eff}}$ method providing stronger net turbulent fluxes (70 W $\mathrm{m^{-2}}$) than the $\mathrm{BA_{pro}}$ method (50 W $\mathrm{m^{-2}}$). In 2009 the SF conditions were frequent and were characterized by warmer air and higher wind speeds than the SF conditions of 2006 (Table 2). Strong forcing conditions were most of the time characterized by high TKE. In these cases low-frequency oscillations, originating from large-scale orographic disturbances and transporting TKE in the surface layer that did not scale with the mean vertical gradients, led to an underestimation of the turbulent fluxes by the $\mathrm{BA_{pro}}$ method (Sect. 4.2). Data from the 2006 campaign showed that the $\mathrm{BA_{eff}}$ method corrected for this effect. This might be the case in 2009, nevertheless, both SEB estimates lie in the uncertainty range of the observed melt.

5.3 Weather patterns

The analysis of meteorological conditions and wind regimes shows that using the WP decomposition of Garavaglia et al. (2010) can be useful to assess turbulent surface fluxes characteristics. The WP analysis is helpful in identifying different kind of circulations in the valley: for WF conditions local thermal winds such as katabatic flows drive the circulation whereas in SF the circulation is dominated by large-scale flows. It also provides a rough classification of the turbulence conditions in the glacier surface-layer, since SF and WF conditions are, in the glacier surface layer, likely associated with high and low TKE conditions, respectively. We show that the BA method compared differently with the EC method for different WP. More generally for SEB studies, we highlight some limitations. For weak forcing conditions only one WP is used which is always associated with weak wind speeds on the glaciers, but for which temperature and cloud cover can be significantly different. The SF conditions are generally characterized by strong winds and cloud covered conditions on the glacier, but can be associated with either cold or warm air flows.

6 Conclusions

During the summers of 2006 and 2009, field measurement campaigns were undertaken in the ablation zone of Saint-Sorlin Glacier, in the French Alps. We analysed Eddy-Covariance data from the 2006 campaign and temperature and wind-speed vertical profiles from the 2009 campaign. We characterized the wind regimes and associated surface-layer turbulent flows, in relation to the large scale forcing as characterized from the weather pattern decomposition of Garavaglia et al. (2010). We evaluated the turbulent fluxes with the bulk aerodynamic (BA) method using observed and melt-calibrated roughness parameters and the Eddy-Covariance (EC) method. We also calculated the surface energy balance and studied the impact of the choice of flux calculation methods on the modeled melt, in relation with weather patterns.

The sensible heat fluxes (H) were warming the surface, they were generally larger in magnitude than latent heat fluxes (LE) which were, on average, a small loss of energy for the glacier. When synoptic forcing was weak, local thermal effects drove the valley wind circulation. A katabatic wind-speed maximum was frequently observed at low height on the glacier (around 2 m, 71% of WF conditions). The turbulent kinetic energy (TKE) was generally low (< 1 m^2 s^{-2}, 68% of the cases), and both H and LE remained small in magnitude. When synoptic forcing was strong, under the influence of low-pressure systems, the large-scale winds roughly aligned with the glacier flow and drove the wind circulation. High wind speeds were observed on the glacier, the TKE was generally high (> 2 m^2 s^{-2}, 52% of the cases) and the katabatic wind-speed maximum was not frequently observed below 5 m (<40% of the time). Sensible heat fluxes were high (>100 W m^{-2}) in these conditions, due to high wind speeds. The magnitude of negative latent heat fluxes, mainly evaporation ($LE < 0$) increased only moderately since the air remained humid, and LE did not cancel the energy gain due to H, so the net flux ($H + LE$) was highly positive.

For all conditions, low-frequency oscillations were observed in the wind-speed signals. When TKE was low, as often observed for weak synoptic forcing, this was likely due to oscillations of the katabatic flow. When TKE was high, as frequently seen for strong synoptic forcing, this was likely due to large-scale orographic disturbances. Former studies in similar context (Smeets et al., 1999; Litt et al., 2015b) suggest that in these cases, TKE transport is non-negligible and that the surface layer

turbulence is not in equilibrium with local turbulence production. These low-frequency oscillations influenced the turbulent momentum and heat fluxes in the surface layer. The non-equilibrium of the surface-layer led to erratic discrepancies between EC fluxes and BA fluxes when TKE was low (Section 5.1). The mean turbulent fluxes calculated with both methods tended to be similar, since the differences between them compensated when averaged over several runs. A systematic underestimation of the EC fluxes by the BA fluxes was observed when TKE was large, which could not be attributed to random measurement errors. As a result the BA fluxes were significantly smaller in magnitude than the EC fluxes.

Surface energy balance calculations compared well to the observed melt. During the 2006 campaign, using turbulent fluxes from the BA or from the EC method did not provide significantly different results. The weather during that campaign was dominated by anticyclonic circulations and weak large-scale forcing. Hence, the turbulent fluxes from both methods were small and not significantly different on average. During the 2009 campaign, many low-pressure systems, associated with strong and warm winds were reported, and turbulent fluxes from the BA method were much larger than during 2006 SF events. The turbulent fluxes calculated with $\mathrm{BA_{pro}}$ underestimated the fluxes calculated with $\mathrm{BA_{eff}}$. Considering the conditions were similar to that observed during the SF events of 2006 the $\mathrm{BA_{pro}}$ method could not account for turbulent mixing that did not scale with the mean gradients in the surface layer, this suggests that in frequent warm and windy conditions, systematic biases might affect the BA method and may lead to underestimating the melt rate on alpine glaciers. The use of an effective roughness to calibrate the SEB on the observed melt increases the fluxes and thus can act as a correcting parameter.

Studies covering more melt periods are necessary to better understand how weather patterns relate to the different SEB terms and to better understand the links between large-scale forcing and mass balance in the vicinity of the glaciers, using dedicated variables to drive a weather pattern decomposition. This would help to understand the climatic processes governing inter-annual variations in the melt regimes of the glaciers. Furthermore, the potential turbulent flux biases might impact the total calculated melt significantly, when calculated over long periods. Turbulent flux error studies would be necessary on other glaciers where turbulent fluxes dominate the SEB, e.g. at high latitudes, such as Storgalciaren (Sicart et al., 2008), or the Canadian artic (Braithwaite, 1981), to assess the effect of these potential biases on melt rate evaluation from climate data.

Acknowledgements. This work was funded by the French SO/SOERE GLACIOCLIM (http://www-lgge.ujf-grenoble.fr/ServiceObs/index.htm) and the ANR program TAG 05-JCJC-0135. We kindly thank EDF for providing the daily time series of WPs. We thank Romain Biron and Jean-Philipe Chazarin for the technical and field work, and Adrien Gilbert and Marion Reveillet for stimulating discussions.

References

Andreas, E.: Parameterizing Scalar Transfer over Snow and Ice: A Review., Jour. Hydrometeorol., 3, 417–432., 2002.

Braithwaite, R. J.: On glacier energy balance, ablation, and air temperature, Journal of Glaciology, 27, 381–391, 1981.

Businger, J. A., Wyngaard, J. C., Izumi, Y., and Bradley, E. F.: Flux-Profile Relationships in the Atmospheric Surface Layer, J. Atmos. Sci., 28, 181–189, 1971.

Conway, J. and Cullen, N.: Constraining turbulent heat flux parameterization over a temperate maritime glacier in New Zealand, Annals of Glaciology, 63, doi:10.3189/2012AoG63A604, 2013.

Corti, S., Molteni, F., and Palmer, T.: Signature of recent climate change in frequencies of natural atmospheric circulation regimes, Nature, 398, 799–802, 1999.

Cullen, N., Mölg, T., Kaser, G., Steffen, K., and Hardy, D.: Energy-balance model validation on the top of Kilimanjaro, Tanzania, using eddy covariance data., Annals of Glaciology, 46, 227–233, 2007.

Denby, B. and Greuell, W.: The use of bulk and profile methods for determining surface heat fluxes in the presence of glacier winds., Journal of Glaciology, 46, 445–452, 2000.

Durand, Y., Brun, E., Merindol, L., Guyomarc'h, G., Lesaffre, B., and Martin, E.: A meteorological estimation of relevant parameters for snow models, Annals of Glaciology, 18, 65–71, 1993.

Dyer, A.: A review of flux-profile relationships., Boundary-Layer Meteorol., 3, 363–372, 1974.

Favier, V., Wagnon, P., and Ribstein, P.: Glaciers of the outer and inner tropics: A different behaviour but a common response to climatic forcing, Geophys. Res. Lett., 31, L16 403, 2004.

Garavaglia, F., Gailhard, J., Paquet, E., Lang, M., Garçon, R., and Bernardara, P.: Introducing a rainfall compound distribution model based on weather patterns sub-sampling, Hydrol. Earth. Syst. Sc., 14, 951–964, 2010.

Gellens-Meulenberghs, F.: Sensitivity Tests of an Energy Balance Model to Choice of Stability Functions and Measurement Accuracy, Boundary-Layer Meteorol., 115, 453–471, 2005.

Helgason, W. and Pomeroy, J.: Problems Closing the Energy Balance over a Homogeneous Snow Cover during Midwinter, J. Hydrometeorol., 13, 557–572, 2012.

Hock, R.: Temperature index melt modelling in mountain areas, Journal of Hydrology, 282, 104–115, 2003.

Højstrup, J.: Velocity Spectra in the Unstable Planetary Boundary Layer, J. Atmos. Sci., 39, 2239–2248, 1982.

Huss, M., Hock, R., Bauder, A., and Funk, M.: 100-year mass changes in the Swiss Alps linked to the Atlantic Multidecadal Oscillation, Geophysical Research Letters, 37, 2010.

Högström, U., Hunt, J. C. R., and Smedman, A. S.: Theory and Measurements for Turbulence Spectra and Variances in the Atmospheric Neutral Surface Layer., Boundary-Layer Meteorology, 103, 101–124, 2002.

Kaimal, J., Wyngaard, J., Izumi, Y., and Coté, O. R.: Spectral characteristics of surface-layer turbulence., Quart. J. Roy. Meteor. Soc., 417, 563–589, 1972.

Litt, M., Sicart, J. E., and Helgason, W. D.: A study of turbulent fluxes and their measurement errors for different wind regimes over the tropical Zongo glacier during the dry season., Atmos. Meas. Tech., 8, 3229–3250, 2015a.

Litt, M., Sicart, J. E., Helgason, W. D., and Wagnon, P.: Turbulence Characteristics in the Atmospheric Surface Layer for Different Wind Regimes over the Tropical Zongo Glacier (Bolivia, 16° S), Boundary-Layer Meteorol., pp. 1–25, doi:10.1007/s10546-014-9975-6, 2015b.

Mahrt, L.: Bulk formulation of surface fluxes extended to weak-wind stable conditions, Quart. J. Roy. Meteor. Soc., 134, 1–10, 2008.

Mann, J. and Lenschow, D. H.: Errors in airborne flux measurements, J. Geophys. Res., 99, 14 519–14 526, 1994.

McNider, R. T.: A Note on Velocity Fluctuations in Drainage Flows, J. Atmos. Sci., 39, 1658–1660, 1982.

Monin, A. and Obukhov, A.: Basic laws of turbulent mixing in the surface layer of the atmosphere, Tr. Akad. Nauk SSSR Geophiz. Inst., 24, 163–187, 1954.

Oerlemans, J.: Glaciers and climate change, CRC Press, 2001.

Oerlemans, J., Giesen, R., and Van den Broeke, M.: Retreating alpine glaciers: increased melt rates due to accumulation of dust (Vadret da Morteratsch, Switzerland), Journal of Glaciology, 55, 729–736, 2009.

Oke, T.: Boundary Layer Climates, 2nd ed., Routeledge, New York, 1987.

Paterson, W. S. B. and Cuffey, K. M.: The physics of glaciers, vol. 3, Pergamon Oxford, 1994.

Pellicciotti, F., Buergi, C., Immerzeel, W. W., Konz, M., and Shrestha, A. B.: Challenges and Uncertainties in Hydrological Modelin of Remote Hindu Kush-Karakoram-Himalayan Basins: Suggestions for Calibration Strategies, Mountain Research And Development, 32, 39–50, 2012.

Poulos, G. and Zhong, S. S.: An Observational History of Small-Scale Katabatic Winds in Mid-Latitudes, Geography Compass, 2, 1798–1821, 2008.

Schotanus, P., Nieuwstadt, F., and Bruin, H.: Temperature measurement with a sonic anemometer and its application to heat and moisture fluxes, Boundary-Layer Meteorol., 26, 81–93, 1983.

Sicart, J., Hock, R., and Six, D.: Glacier melt, air temperature, and energy balance in different climates: The Bolivian Tropics, the French Alps, and northern Sweden, J. Geophys. Res., 113, D24 113, 2008.

Sicart, J. E., Litt, M., Helgason, W., Tahar, V. B., and Chaperon, T.: A study of the atmospheric surface layer and roughness lengths on the high-altitude tropical Zongo glacier, Bolivia, J. Geophys. Res. Atmos., 119, 3793–3808, 2014.

Six, D. and Vincent, C.: Sensitivity of mass balance and equilibrium-line altitude to climate change in the French Alps, Journal of Glaciology, 60, 867–878, 2014.

Six, D., Wagnon, P., Sicart, J., and Vincent, C.: Meteorological controls on snow and ice ablation for two contrasting months on Glacier de Saint-Sorlin, France, Ann. Glaciol., 50, 66–72, 2009.

Smeets, C. and Van den Broeke, M.: The parameterisation of scalar transfer over rough ice, Boundary-layer meteorology, 128, 339–355, 2008a.

Smeets, C., Duynkerke, P., and Vugts, H.: Observed wind profiles and turbulence fluxes over an ice surface with changing surface roughness, Boundary-Layer Meteorol., 92, 99–121, 1999.

Smeets, C., Duynkerke, P., and Vugts, H.: Turbulence characteristics of the stable boundary layer over a mid-latitude glacier. Part II: Pure katabatic forcing conditions, Boundary-layer Meteorol., pp. 73–107, 2000.

Smeets, C. J. P. P. and Van den Broeke, M. R.: Temporal and Spatial Variations of the Aerodynamic Roughness Length in the Ablation Zone of the Greenland Ice Sheet, Boundary-Layer Meteorol., 128, 315–338, 2008b.

Stoy, P. C., Mauder, M., Foken, T., Marcolla, B., Boegh, E., Ibrom, A., Arain, M. A., Arneth, A., Aurela, M., Bernhofer, C., Cescatti, A., Dellwik, E., Duce, P., Gianelle, D., van Gorsel, E., Kiely, G., Knohl, A., Margolis, H., McCaughey, H., Merbold, L., Montagnani, L., Papale, D., Reichstein, M., Saunders, M., Serrano-Ortiz, P., Sottocornola, M., Spano, D., Vaccari, F., and Varlagin, A.: A data-driven analysis of energy balance closure across FLUXNET research sites: The role of landscape scale heterogeneity, Agric. For. Meteorol., 171-172, 137–152, 2013.

Stull, R.: An Introduction to Boundary Layer Meteorology, Springer, Netherlands, 1988.

Vickers, D. and Mahrt, L.: Quality Control and Flux Sampling Problems for Tower and Aircraft Data, J. Atmos. Oceanic Technol., 1, 512–526, 1997.

Vincent, C., Vallon, C., Reynaud, L., and Meur, E. L.: Dynamic behaviour analysis of glacier de Saint Sorlin, France, from 40 years of observations, 1957–97, Journal of Glaciology, 46, 499–506(8), 2000.

Viviroli, D., Archer, D. R., Buytaert, W., Fowler, H. J., Greenwood, G. B., Hamlet, A. F., Huang, Y., Koboltschnig, G., Litaor, M. I., López-Moreno, J. I., Lorentz, S., Schädler, B., Schreier, H., Schwaiger, K., Vuille, M., and Woods, R.: Climate change and mountain water resources: overview and recommendations for research, management and policy, Hydrology and Earth System Sciences, 15, 471–504, 2011.

Wagnon, P., Sicart, J. E., Berthier, E., and Chazarin, J. P.: Wintertime high-altitude surface energy balance of a Bolivian glacier, Illimani, 6340 m above sea level, J. Geophys. Res., 108, 4177, 2003.

Wilckzak, J. M., Oncley, S. P., and Stage, S. A.: Sonic Anemometer Tilt Correction Algorithms, Boundary-Layer Meteorol., 99, 127–150, 2001.

Wyngaard, J.: On surface layer turbulence, in: Haugen, D.A. (Ed.), Workshop on Micrometeorology. American Meteorological Society., 1973.